Spatially Invariant Classification of Tissues in MR Images

Stephen Aylward and James Coggins

Department of Computer Science
University of North Carolina at Chapel Hill

Ted Cizadlo and Nancy Andreasen

Department of Psychiatry
University of Iowa Hospitals and Clinics

ABSTRACT

Inhomogeneities in the fields of magnetic resonance (MR) systems cause the statistical characteristics of tissue classes to vary within the resulting MR images. These inhomogeneities must be taken into consideration when designing an algorithm for automated tissue classification. The traditional approach in image processing would be to apply a gain field correction technique to remove the inhomogeneities from the images. Statistical solutions would most likely focus on including spatial information in the feature space of the classifier so that it can be trained to model and adjust for the inhomogeneities.

This paper will prove that neither of these general approaches offers a complete and viable solution. This paper will in fact show that not only do the inhomogeneities modify the local mean and variance of a tissue class as is commonly accepted, but the inhomogeneities also induce a rotation of the covariance matrices. As a result, gain field correction techniques cannot compensate for all of the artifacts associated with inhomogeneities. Additionally, it will be demonstrated that while statistical methods can capture all of the anomalies, the across patient and across time variations of the inhomogeneities necessitate frequent and time consuming retraining of any Bayesian classifier.

This paper introduces a two stage process for MR tissue classification which addresses both of these issues by utilizing techniques from image processing and statistics. First, a band-pass mean field corrector is used to compensate for the mean and variance deformations in each image. Then, using a kernel mixture model classifier coupled to an interactive data augmentation tool, the user can selectively refine and explore the class representations for localized regions of the image and thereby capture the rotation of the covariance matrices. This approach is shown to outperform Gaussian classifiers and 4D mixture modeling techniques when both the final accuracy and user time requirements are considered.

1. INTRODUCTION

A magnetic resonance (MR) imaging system measures the magnitude and relaxation rate of the induction field generated by a sample when the axis of proton spin of a portion of its atoms become partially aligned by a strong magnetic field. It is a complex and sensitive process by which these fields are maintained and measured. Variations in sample density, coil quality, and even room temperature are just some of the factors which can adversely affect the consistency of the fields and thereby produce spatial correlations (inhomogeneities) in the recorded values.[1,2] These inhomogeneities are seen as "shadings" or intensity gradients in the displayed MR images. These intensity variations usually do not affect the visual diagnosis process of the radiologist. Yet, these intensity variations interfere with the automated labeling of MR imaged tissues using spatially invariant classifiers.[1,2,3,4,5] The development of a spatially invariant tissue classification system has the potential to expand the useful lifetime of older equipment and reduce the cost of manufacturing and maintaining newer equipment.

Techniques from two schools of thought have been applied to this problem. Image processing suggests a gain field correction technique to remove the inhomogeneities.[2,4] Statisticians suggest including spatial information in the feature space so that the classifier can be trained to model the statistically correlated deformations and thus take them into consideration when producing a labeling.[1]

This paper explores the effect of MR inhomogeneities on the statistical characteristics of the white matter, gray matter, cerebrospinal fluid, and background classes. It provides quantitative proof that the tissue covariance matrices do undergo a rotation within the inhomogeneities which cannot be compensated for using bias correction. It also demonstrates how the MR inhomogeneities can vary across patients, time, and slices (Z axis) thereby requiring user intensive training data collection for each MR run when Bayesian methods are employed.

As an alternative approach to this problem, this paper presents a solution which requires minimal training data, is robust across patients and time, and which provides the user an intuitive tool for the exploration and refinement of the spatially localized class representations. It combines a gain field correction technique with a kernel mixture model classifier which supports interactive data augmentation.[6] This approach is compared with Gaussian classifiers[7,5] and 4D mixture modeling techniques[8,1]. Classification accuracy of these systems is quantified whenever possible. Training data requirements are also considered. Given multiple MR runs it is shown that the mean field kernel mixture model classifier offers the best performance.

2. DATA COLLECTION AND PROCESSING

All data used for this paper was collected on a 1.5 Tesla GE MRI system at the University of Iowa. Specifically, seven data sets were used. They can be grouped as runs from : same person different day, different person same day, and different person different day. Each data set is comprised of 57-58, 3 mm thick, continuous, coronal, PD and T2 slices. For each data set, MR parameters were chosen so as to offer the best separation of gray and white matter. Because of the variations in the inhomogeneities, different data sets often had different MR parameters.

In order to suppress the high frequency noise inherent in the images while preserving the sharp edges, variable conductance diffusion is applied.[9] This algorithm uses gradient information from both the PD and T2 images to control the diffusion process. Twenty iterations were run with conductance = 3 and $\sigma = 0.6$ so that small image structures are preserved. The end result is an improvement in the separation and variance of the tissue classes in feature space. This process provides only minimal compensation for the intensity distortion.

3. TRAINING AND TESTING DATA

This paper focuses on the data from two of the MR runs :

Data set A was recorded on December 4, 1992. It contains 57 coronal PD and T2 slices. The magnitude of the inhomogeneity in this data set proved to be the strongest among the seven data sets available. Slices A12, A20, and A28 provided the 5,210 training data points. All four classes (cerebrospinal fluid, gray matter, white matter, and background) were represented. These points were used in training the Gaussian and 4D mixture modeling approaches and were used to determine the expected class statistics for the kernel mixture model classifier. These points were not selected as continuous regions in the image, but were selected individually or in small circular regions of radius 1 - 3 pixels. Special emphasis was placed on maintaining nearly uniform training data sampling across each slice. Slice A25, shown in Figures 1 and 2, was the "same-run" testing data. The magnitude of the inhomogeneity is noticeable in the image as a dimming in the inferior cerebellum. From this slice 2,515 points were hand selected to quantify the testing performance of each algorithm. These points were chosen so as to be strong exemplars of their associated classes. However, in order to better discriminate between the algorithms, the testing points were heavily

concentrated in the areas of the inhomogeneities.   As with the training pixels, these points were selected individually or in small circular regions of radius 1 - 3 pixels.
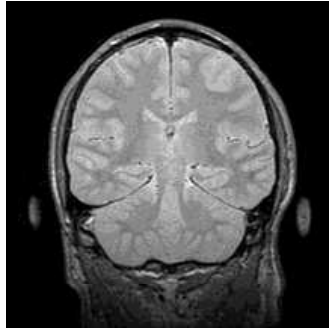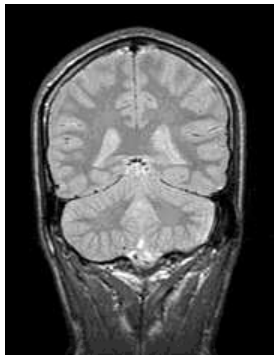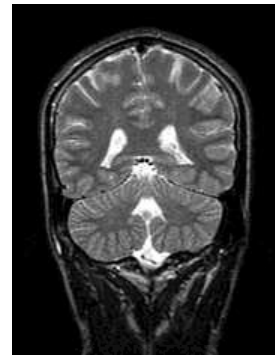

PD Image from testing slice A25.
Figure 1
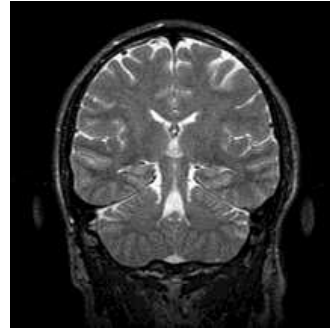
T2-weighted Image from testing slice A25.
Figure 2

Data set B was recorded from a different patient than data set A on July 2, 1993.   It consists of 57 PD and T2 coronal slices.   Slice B20 was selected as a testing slice (shown in Figures 3 and 4).   The location of the inhomogeneity is nearly the same as the one in data set A, however its magnitude is significantly less. No training data was selected from this run.   Also, no hand labelings were available to quantify performance differences, but it will be shown that a cursory visual inspection is more than sufficient to discriminate between the algorithms' performance.

PD Image from testing slice B20.
Figure 3

T2-weighted Image from testing slice B20.
Figure 4

Thus, the three training slices (A12, A20, and A28) and two testing slices (A51 and B20) provide a means to test each algorithms performance under the simplest (same run training and testing) and the most difficult (different people on different days training and testing) conditions.   Gray matter proved to be the most difficult of the four classes to accurately segment.   Partial voluming and its proximity to the white matter cluster in feature space were two major contributors to its poor labeling accuracy. As a result, the quantification of the performance of the algorithms uses the false positive and true positive rates for the gray matter.   These rates are determined by comparing the automated labelings with the hand labelings for the select testing pixels from A25.
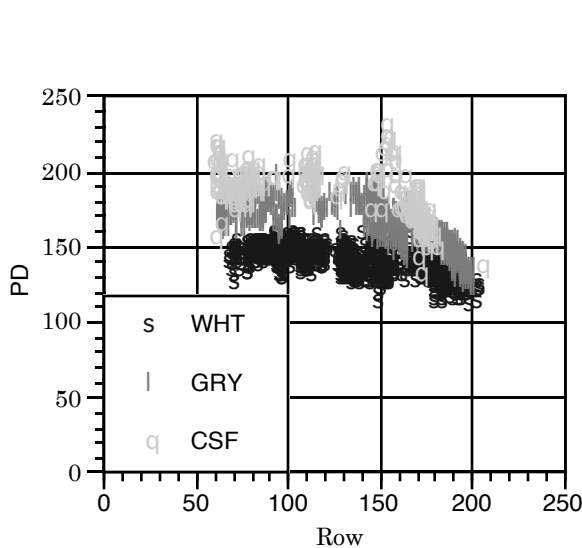
4. MR INHOMOGENEITIES

Included in the list of causes of MR inhomogeneities are poor coil quality, variations in matter density in and near the sample being imaged (e.g. dental work), and inappropriate MR parameter settings/tuning. The following facts about MR inhomogeneities are commonly accepted :

- MR inhomogeneities affect the local mean value of the tissue classes
- MR inhomogeneities affect the local magnitude of the variance of the classes
- MR inhomogeneities change across patients, time, and slices (Z axis)
- MR inhomogeneities affect different echoes differently

This paper demonstrates that :

- MR inhomogeneities cause a rotation of the covariance matrices for the tissue classes

Figure 5 shows a PD/Row scattergram of the hand labeled testing pixels. It illustrates the change in the local mean and variance magnitude for each class at the inhomogeneity (beginning about row 175). If Gaussians are fit to the distribution of the PD/T2 sample values from each class then the isoprobability curves in the PD/T2 feature space can be plotted (Figure 6). Notice the poor separation of the gray and white matter classes.

PD-versus-Row scattergram
of the testing data (A25)
Figure 5
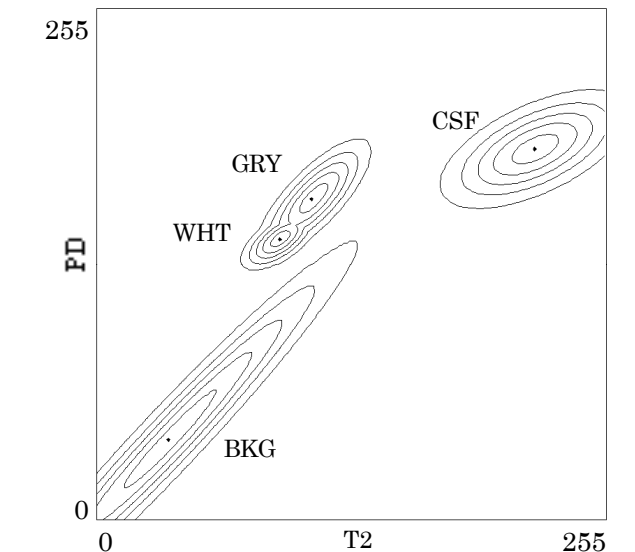
Isoprobability curves of approximated PD-versus-
T2 distribution of the testing data (A25)
Figure 6

The effect of the inhomogeneity can be better visualized by separately viewing the statistical characteristics of samples contained within the inhomogeneity and comparing them with samples from "outside" the inhomogeneity (referred to as homogeneous data). This separation is achieved by splitting each tissue class into two subclasses (inhomogeneous versus homogeneous) based on the spatial bounds of the inhomogeneity (row 175). When the isoprobability curves for the gray matter subclasses are plotted, Figure 7 results. It clearly portrays the change in the mean and variance associated with the inhomogeneity. Notice also that this plot reveals a change in the orientation of the covariance matrix as a function of the inhomogeneity. Similar warpings occur for the white matter and cerebrospinal fluid classes.

By calculating the maximum eigenvalued eigenvector of a covariance matrix, the principal direction of the variance of its data can be determined. Table 1 contains a summary of the directions of the maximum eigenvalued eigenvectors for the gray matter classes and subclasses. It further illustrates the effect of the inhomogeneities on the orientation of the covariance matrix.
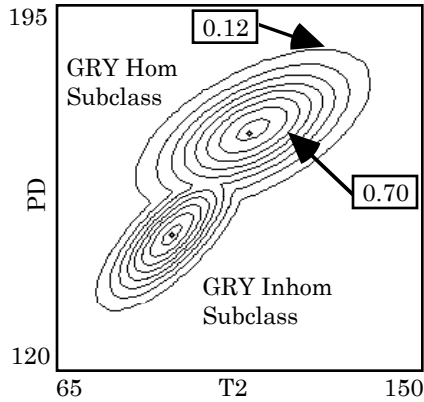
Isoprobability curves of gray matter
subclasses in subrange of PD/T2 feature space
Figure 7

Portion of Gray Matter	Direction of Max Variance (degrees)
All Gray Matter Data	46.086
Homogeneous Subclass	60.186
Inhomeneous Subclass	47.290

Directions of maximum eigenvalued eigenvector
of covariance matrices
Table 1

5. PREVIOUS WORK

5.1 Gaussian Classifiers

MR tissue classifiers usually operate in the two dimensional feature space defined by the PD and T2 measurements. Gaussian distributions are fit to this data by calculating each class' mean and covariance matrix based on the distribution of the training data samples. Testing pixels are assigned the label which has the maximum likelihood for their particular combination of PD and T2 values.
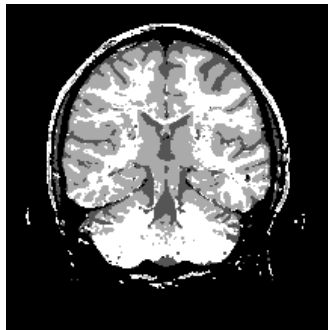
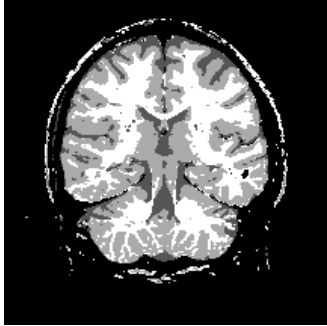Labeling of A25 by Gaussian classifier
Figure 8
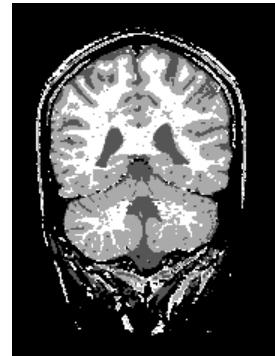
Labeling of B20 by Gaussian classifier
Figure 9

Figures 8 and 9 illustrate the labelings generated for the two testing slices via the Gaussian classification method. Notice how the inhomogeneities produce numerous misclassifications in the cerebellum in both cases. Comparing these labelings with the hand labeled gray matter pixels, a false positive rate of 9.96% and a true positive rate of 68.19% resulted. Obviously, neither the changes in the mean nor the changes in the covariance matrix resulting from the inhomogeneities can be captured by this spatially invariant process.
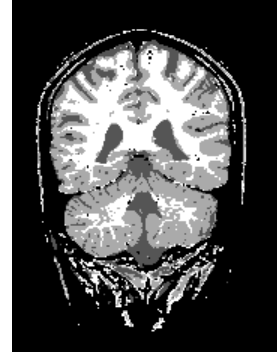
5.2 4D Mixture Modeling

By adding spatial information (Row, Column) to the feature vectors associated with each pixel, a 4D feature space can be created (PD, T2, Row, Column). Mixture modeling then uses an expectation-maximization algorithm to fit multiple Gaussians to each class so as to better represent each class and the changes it undergoes as a result of the inhomogeneity. Using the same training data, this technique produces the

results shown in Figures 10 and 11. Notice how the gray and white matter is well differentiated in the cerebellum in A25. Comparing these labelings with the hand labeled gray matter testing pixels, a much improved false positive rate of 3.76% and a true positive rate of 93.03% were attained.

Labeling of A25 by 4D mixture model classifier

Figure 10

Labeling of B20 by 4D mixture model classifier

Figure 11

Figure 10 suggests that this technique is able to capture both the change in the mean and the rotation of the covariance matrix for test images originating from the same MR run as the training data. However, Figure 11 clearly shows that this technique will not work across patients and time. In fact, even the usually less severe Z axis (slice by slice) changes to the inhomogeneities which occur within a single run can affect this classifier's performance. Thus, frequent, user intensive retraining is necessary, and the requirement of a large amount of spatially well distributed training data (to avoid biasing the individual models in the mixture) makes the retraining process especially cumbersome and time consuming.

6. THE SOLUTION

In order to accurately compensate for all of the anomalies introduced by the inhomogeneities without requiring retraining, a two step algorithm is suggested : a band-pass mean field correction followed by a kernel mixture model classifier coupled with an interactive data augmentation tool.

6.1 Band-Pass Mean Field Correction

The band-pass mean field correction is dedicated to adjusting the image for the change in the class means and variance magnitudes which result from the inhomogeneities. One of the obvious manifestations of the inhomogeneities is a localized change in mean tissue value. Our work revealed that the background class is basically unaffected by the inhomogeneity. Additionally, we discovered that the ratio of the warped local mean of a class to that class' global mean is equal to the ratio of that classes warped variance to its global variance (where the variance is defined by the eigenvalues of the covariance matrix). Thus, only the deformations to the local mean need to be tracked in order to correct both of these anomalies.

There are two main steps in correcting for gain in an image. The first step involves estimating the mean field for the image. The second step uses the ratio of local mean to the global mean to determine the multiplicative correction coefficient for that local region. Due to the inconsequent of the background class in tracking the deformations and in an effort to limit the effect of image structure on calculating the local mean, a band-pass mean field estimator was used. So, in order to calculate the mean field value at a pixel, all pixels within a 30 pixel radius are consider, however, only those pixels whose value is greater than 40 actually contribute to the estimate of the local mean. Figures 12 and 13 show a level curve plot of the local mean field for the A25 testing slice. It is important to note that different echoes have different mean field configurations. Also, by observing the contour plots from a sequence of the slices, the smooth variations of the mean field across the slices becomes clear.
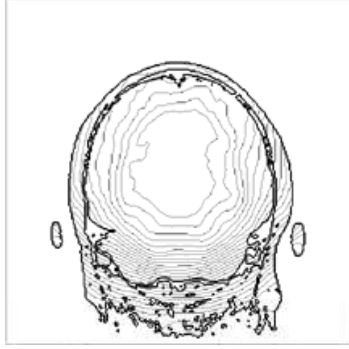
Contour plot of the PD mean field value,
$M_{PD}(r,c)$, for A25

Figure 12
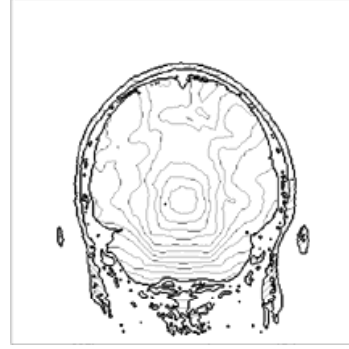
Contour plot of the T2 mean field value,
$M_{T2}(r,c)$, for A25

Figure 13

Once the mean field has been estimated, the local multiplicative correction coefficient is calculated as the ratio of the global mean field value to the local mean field value. Thus, when individual pixel values are multiplied by this coefficient, their local mean is adjusted so that it more closely matches a global mean. The result of performing this processing on the A25 testing data is shown in Figures 14 and 15. As expected, there is a general brightening and contrast enhancement in the inferior cerebellum as the mean and variance deformations due to the inhomogeneity are eliminated (compare with Figures 1 and 2).
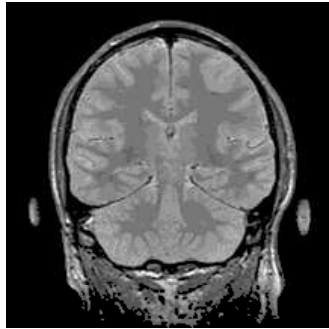
Band-pass mean field corrected A25-PD

Figure 14
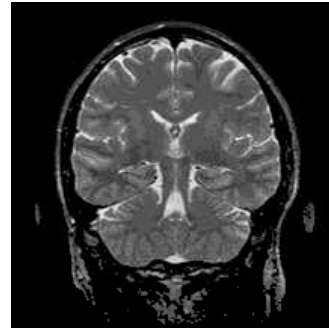
Band-pass mean field corrected A25-T2

Figure 15
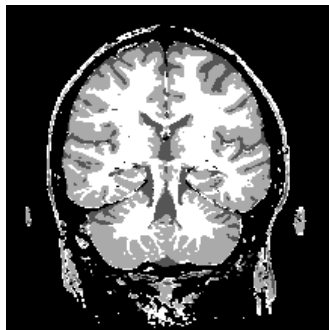
Gaussian labeling of corrected A25-PD/T2

Figure 16

Gaussian labeling of corrected B20-PD/T2

Figure 17

A standard Gaussian classifier can be applied to these images in the same manner as before. The resulting labelings for the two test images are shown in Figures 16 and 17. The associated false positive rate is 2.14% and the true positive rate is 95.06% and no retraining is required across patients, time, or Z axis. This is a significant improvement over the classification accuracy and work requirements associated

with the application of a Gaussian classifier or the 4D mixture model classifier to the unprocessed data (see Figures 8, 9, 10, and 11). However, neither the band-pass mean field corrections nor the PD/T2 based Gaussian classifier is able to adjust for the rotation of the covariance matrix.

The effect of the inhomogeneity on the orientation of the covariance matrix can now be seen even more clearly. It is best shown by viewing the isoprobability curves of the subclasses (inhomogeneous versus homogeneous) of the testing data as was done for the uncorrected gray matter in Figure 7. This plot is shown in Figure 18. Additionally, the direction of maximum variance for the processed data can be calculated from the eigenvectors of the covariance matrix as was done in Table 1, thus producing Table 2. Although there is now better correspondence in the location of the subclass means and in the magnitude of their variances, the rotation of the covariance matrices across the subclasses is still clearly visible. A statistical method other than a Gaussian classifier must be applied in order to model and compensate for this remaining spatially correlated anomaly while not introducing significant training requirements.
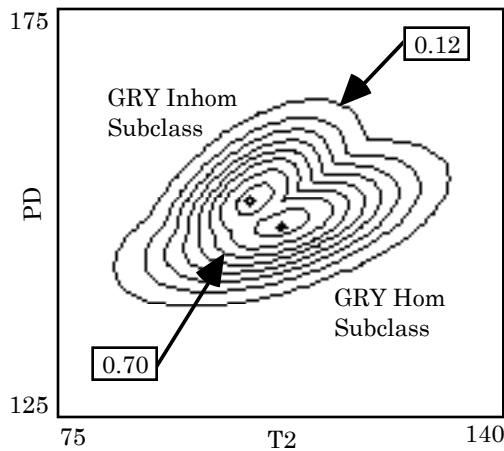
Isoprobability curves of the estimated distribution
of the A25 subclasses in PD versus T2 feature space
Figure 18

Portion of Gray Matter	Direction of Max Variance (degrees)
All Gray Matter Data	69.871
Homogenious Subclass	72.411
Inhomogeneity Subclass	38.521

Directions of max eigenvalued eigenvector
of covariance matrix
Table 2

6.2 Kernel Mixture Modeling with Data Augmentation

The application of kernel mixture models to inhomogeneous image data is intuitive. Instead of associating a local mean field value with each pixel, a complete Gaussian classifier is associated with each pixel (or small group of localized pixels, "a kernel"). By initializing all of these Gaussian classifiers with the statistical characteristics of the training data, the same labeling will result for the testing data as if a single Gaussian had been used. Our implementation of the kernel mixture modeling algorithm provides improved results once it is combined with an interactive data collection/augmentation system. Given an initial labeling of an inhomogeneous image, the user selectively modifies the statistical characteristics of the kernel mixtures associated with a localized region of the image by simply revising or emphasizing the labeling at a point of interest. Thus, changes in tissue class means, variances, and even covariance matrix orientation can be applied by interactively correcting misclassifications or reinforcing correct labelings.

Specifically, when the user clicks on a single pixel to indicate its membership in a particular class (which may revise or reinforce the current labeling), the mean and covariance matrices of the corresponding class at the kernels near that pixel are modified. The nearer (in image space) the indicated pixel is to a kernel, the more influence its data values have on that kernel's statistics. The algorithms for modifying the class statistics are simply those used for tracking the mean and variance of sequentially arriving data. The strength of the influence is controlled by increasing the assumed number of prior training points (the assumed sample population) as the distance to the indicated pixel increases.

Experience has shown that very few point clicks (10-15) are required to significantly improve the classification results.   The system's response time is under 1 second, so very little user time is required for this amount of interaction.   Figures 19 and 20 show the final classifications achieved using the complete mean field kernel mixture modeling with interactive data augmentation.   Less than 20 pixel selections were necessary to achieve each of these labelings.   The associated false positive rate is 0.98% and the true positive rate is 94.42%.   Considered together, these rates are the best of all of the algorithms presented.

It should also be noted, that this tool greatly facilitates the exploration of the structures of the brain.   For example, striations in the cerebellum, many of which are barely visible, can be interactively explored (followed) as the sensitivity of the local classifiers is modified.   Additionally, the handling of partial voluming can be localized to aid in the detection of even more subtle structures such as the basal nuclei.
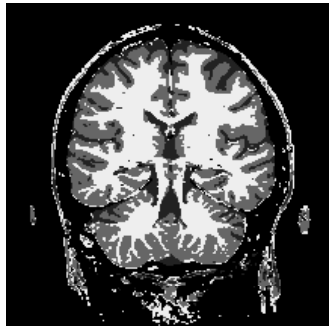
Final labeling of A25 using the mean field kernel mixture modeling technique
Figure 19
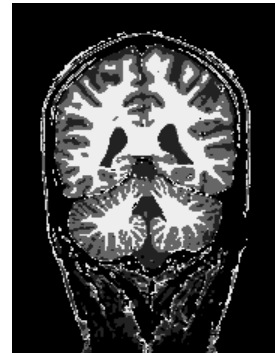
Final labeling of B20 using the mean field kernel mixture modeling technique
Figure 20

7. CONCLUSION AND FUTURE WORK

Thus, MR inhomogeneities affect not only the mean and variance of the tissue classes, but also the orientation of the covariance matrix.   Digital filtering or statistical methods alone do not produce viable solutions to these problems.   However, by utilizing techniques from both schools of thought, a robust solution can be achieved.

Current work is focusing on understanding the cause and developing a mathematical representation of the covariance rotation which results from the inhomogeneities.   Other work is concentrating on developing logical constraints on the modifications which can occur to the kernel mixtures as a result of data augmentation.   It is hoped that additional constraints will facilitate the convergence of the classifiers.

8. REFERENCES

1. Aylward, S., Coggins, J., Cidzadlo, T., and Andreason, N., "The Effects of Magnetic Resonance Image Inhomogeneities on Automated Tissue Classification," *AAAI Spring Symposium on Applications of Computer Vision to Medical Image Processing*, 1994

2. Wells, W., Grimson, W., Kikinis, R., and Jolesz, F., "Statistical Gain Correction and Segmentation of MRI Data," *IEEE Computer Vision and Pattern Recognition Conference*, 1994

3. Cohagan, J., et al., "Multispectral Analysis of MR Images of the Breast," *Radiology*, Vol. 163, 1987

4. Dawant, B., Zijdenbos, A., Margolin, R., "Correction of Intensity Variations in MR Images for Computer-Aided Tissue Classification," *IEEE Transactions on Medical Imaging*, Vol. 12, No. 4, December 1993

5. Gerig, G., et al., "Automating Segmentation of Dual-Echo MR Head Data," *Information Processing in Medical Imaging*, Springer-Verlag, 1991

6. Titterington, D., Smith, A., and Makov, U., <u>Statistical Analysis of Finite Mixture Distributions</u>, John Wiley and Sons, Chichester, 1985

7. Duda, R., and Hart, P., <u>Pattern Classification and Scene Analysis</u>, John Wiley and Sons, New York, 1973

8. McLachlan, G. and Basford, K., <u>Mixture Models: Inference and Applications to Clustering</u>, Marcel Dekker, INC. 1988

9. Yoo, T., and Coggins, J., "Using Statistical Pattern Recognition Techniques to Control Variable Conductance Diffusion," *Information Processing in Medical Imaging*, Springer-Verlag, 1993